Biophysical Journal
Article

Biophysical Society

DOTAP: Structure, hydration, and the counterion effect

Mihaela Mihailescu,[1,*] David L. Worcester,[2,3,4] Christopher L. Carroll,[5] A. Richard Chamberlin,[5,6] and Stephen H. White[3,4]

[1]Institute for Bioscience and Biotechnology Research, Rockville, Maryland; [2]Biology Division, University of Missouri, Columbia, Missouri; [3]NIST Center for Neutron Research, National Institute of Standards and Technology, Gaithersburg, Maryland; [4]Department of Physiology and Biophysics, University of California at Irvine, Irvine, California; [5]Department of Chemistry, University of California at Irvine, Irvine, California; and [6]Department of Pharmaceutical Sciences, University of California at Irvine, Irvine, California

ABSTRACT The cationic lipid 1,2-dioleoyl-3-trimethylammonium propane (DOTAP) is one of the original synthetic cationic lipids used for the liposomal transfection of oligonucleotides in gene therapy. The key structural element of DOTAP is its quaternary ammonium headgroup that is responsible for interactions with both nucleic acids and target cell membranes. Because these interactions are fundamental to the design of a major class of transfection lipids, it is important to understand the structure of DOTAP and how it interacts with halide counterions. Here, we use x-ray and neutron diffraction techniques to examine the structure of DOTAP and how chloride (Cl^-) and iodide (I^-) counterions alter the hydration properties of the DOTAP headgroup. A problem of particular interest is the poor solubility of DOTAP/I^- in water solutions. Our results show that the poor solubility results from very tight binding of the I^- counterion to the headgroup and the consequent expulsion of water. The structural principles we report here are important for assessing the suitability of DOTAP and its quaternary ammonium derivatives for transfection.

SIGNIFICANCE The structure and chemistry of positively charged (cationic) lipids used in nanoparticle formulations dictate, ultimately, their usefulness as carriers for nucleic acids. Common cationic lipids used in gene therapies contain a trimethylammonium motif bound to a counterion, typically, Cl^- or I^-. Our structural study of DOTAP shows that the counterion strongly affects both lipid packing and hydration of DOTAP, meaning that the choice of counterion requires careful consideration when similar lipids are used for transfection.

INTRODUCTION

Cationic lipids are receiving renewed attention due to recent successes with their use in lipid nanoparticle (LNP) formulations for intracellular delivery of therapeutic nucleic acids, particularly COVID-19 mRNA vaccines (1) and siRNA cancer treatments (2). The lipids N-[1-(2,3-dioleoyloxy) propyl]-N,N,N-trimethylammonium chloride (DOTMA) (3) and 1,2-dioleoyl-3-trimethylammonium propane (DOTAP)—an ester analog of DOTMA (4)—are two of the first-generation DNA/RNA transfection reagents. DOTAP has also been found to be a useful tool for studies of voltage-gated ion channels (5,6), due to interesting chemical properties that arise from the positively charged headgroup and lack of a phosphate moiety (Fig. 1). Consequently, DOTAP is an important molecular model for various applications, primarily for transfection.

The suitability of LNPs for therapeutic/vaccine delivery depends on the chemistry and structure of their constituent lipids, which usually consist of the cationic lipid mixed with a "helper lipid"—most typically one carrying a phosphatidylcholine (PC) or phosphatidylethanolamine (PE) headgroup—to achieve increased uptake by the target cells (3,4,7). The LNP cationic lipid, however, plays the central role in transfection through collection/condensation of negatively charged nucleic acids and in the attachment of LNPs to the anionic lipids of target cells. Although many structural variations in both the headgroup region and the alkyl chains have been proposed in numerous attempts to improve transfection efficacy and minimize toxicity, the quaternary ammonium headgroup is by far the most frequently used structural motif in many of the established cationic lipids (8). Consequently, the structural features of

Submitted September 24, 2022, and accepted for publication January 23, 2023.

*Correspondence: ella11@umd.edu

Editor: Sarah Veatch.

https://doi.org/10.1016/j.bpj.2023.01.031

the cationic lipid headgroup region are of particular importance. Physicochemical properties such as surface charge, hydrogen bonding capability, surface hydration, and steric hindrance around the ammonium ion headgroup have all been shown to affect DNA complexation with LNPs and the fusion of the LNPs with the target cell membrane (reviewed by Zhi et al. (8)).

An important issue, rarely acknowledged in transfection studies, is the effect of the counterions used for stabilizing the positively charged lipid headgroups. Of particular interest is the use of iodide in lieu of the more commonly used chloride counterion. The counterion appears to affect transfection, because use of I^- versus Cl^- forms of the same lipid has been shown to alter transfection outcome (9,10), although the trends found are irregular. We suspect that this is because of the differences in water solubilities and bilayer structures of the two halide forms, DOTAP/Cl^- versus DOTAP/I^-. The differences are likely to affect the miscibility of the cationic lipid with helper lipids in liposomal formulations and the actual fraction of cationic lipid incorporated. Because nucleic acids can also bind to zwitterionic lipids used in LNP mixtures, transfection can happen even if a cationic lipid in iodinated form is used, but probably with reduced efficiency or reproducibility. In that case, although the role of the iodinated lipid remains uncertain, the results of transfection studies can vary significantly.

In this study, we found that DOTAP/Cl^- readily forms stable liposomes in water, whereas DOTAP/I^- does not. Similar observations have been reported for a pH-sensitive DOTAP derivative containing an ortho ester group (11), suggesting that the solubility problem is not unique to the trimethylammonium (TMA) group of DOTAP. Because iodinated variants of DOTAP and its derivatives are used for both in vivo and in vitro gene delivery studies (9,12,13), it is important to understand the solubility issue from a structural perspective. To gain insights into the problem, we have carried out structural studies of DOTAP and phospholipid analogs using x-ray and neutron diffraction methods in conjunction with specific deuterium (D = ^{2}H) labeling. We show that DOTAP/Cl^- and DOTAP/I^- show very different hydration behavior, with DOTAP/I^- exhibiting complete dehydration. The insolubility of DOTAP/I^- and the tendency to segregate away from other lipid components in mixed bilayers are important considerations for its usage in transfection.

MATERIALS AND METHODS

Synthesis of N-methyl-trideuterated (S)-DOTAP chloride and iodide

The chloride and iodide salts of (S)-1,2-dioleoyl-3-(d_3-trimethylammonium) propane, for simplicity referred to in the text as deuterated DOTAP or (D3)DOTAP, respectively, were prepared as described by Leventis and Silvus for unlabeled, racemic DOTAP chloride (14). The racemic 3-dimethylamino-1,2-propane diol key intermediate employed in those studies was replaced with (S)-3-dimethylamino-1,2-propane, which was synthesized by minor modification of published procedures (15–17).

In brief, the (S)-3-dimethylamino-1,2-propane diol was prepared by conversion of D-mannitol into D-glyceraldehyde-2,3-acetonide, followed sequentially by 1) direct conversion into the corresponding amide, 2) $LiAlH_4$ reduction to the primary amine, and 3) conversion into (S)-3-dimethylamino-1,2-propane diol via a double reductive amination. After removal of the acetonide protecting group, the resultant diol was treated with a slight excess of oleoyl chloride to form the corresponding 1,2-dioleoyl-3-dimethylamino derivative, which after purification, reacted cleanly with d_3-methyl iodide to produce (D3)DOTAP iodide. A portion of the iodide salt was subjected to iodide-to-chloride exchange (14), and both salts were isolated in pure form after chromatographic purification. The unlabeled DOTAP salts were prepared by the same procedure, but nondeuterated methyl iodide was substituted for d_3-methyl iodide in the methylation of the 1,2-dioleoyl-3-dimethylamino intermediate.

Sample preparations

DOTAP/Cl^- oriented samples were prepared by depositing a thin film of lipid (~2 mg) on a glass coverslip by thoroughly removing the chloroform under a stream of nitrogen gas followed by reconstitution in water at neutral pH. About 200 μL of a concentrated vesicle suspension (10 mg/mL) in water was fused to thin glass coverslips and the bulk water was allowed to slowly evaporate at room temperature. This procedure resulted in an oriented lipid stack of ~2000 bilayers. DOTAP/I^-, received as a lyophilized powder, was mixed directly with either chloroform, water at neutral pH, a HEPES buffer (20 mmol/L HEPES, 100 mmol/L NaCl, pH 7.2) or a phosphate buffer (10 mmol/L Na_3PO_4, 50mM NaCl, pH 6.8), at target concentrations of 5–10 mg/mL. The lipid readily formed a clear solution in chloroform. When the chloroform was removed under a stream of nitrogen gas, a lipid film was obtained that could not be dispersed in pure water (it remained glued to the glass vial) despite repeated treatments with sonication, heating, and freeze-thaw cycles. When DOTAP/I^- in powder form was mixed directly with pure water, the lipid remained in the form of insoluble particulates, whereas HEPES and phosphate buffer with sodium chloride salts produced milky, white suspensions, which were deposited on glass coverslips to form multilayers. For DOPC/DOTAP/I^- samples, the two lipids were mixed in proportion of 1:1 in chloroform, a solvent in which both of the lipids are individually soluble. The chloroform was then removed, and the lipid film was hydrated from phosphate buffer, which was the same that was used for DOTAP/I^-. Samples in water-based buffers were hydrated over 2 days with intermittent vortexing and repeated treatments with heat (37°C) in a bath sonicator. However, all samples containing DOTAP/I^- had traces of small, waxy particulates that were visible by eye. Mixtures of DOTAP/Cl^- and DOTAP/I^- with DOPC were also prepared from chloroform and water/chloroform mixtures. Before measurements, the oriented samples were equilibrated for several hours in the water vapor of a saturated salt (KNO_3) solution, at a relative humidity (RH) of 93% and room temperature.

Neutron and x-ray diffraction

Diffraction data from oriented samples were obtained under controlled temperature-humidity conditions (23°C, 66%, 86%, 93%, and 98% RH) using the MAGIk instrument at the NIST Center for Neutron Research, Gaithersburg, MD (18). The RH in the sample enclosure was controlled by changing the partial vapor pressure with various saturated salt solutions (19).

Bragg diffraction peaks were collected from (h,0,0) planes, probing the direction normal to the bilayer surface. Bilayer structure factors were determined as the square root of the integrated intensities of the Bragg peaks, corrected for background, absorption, and extinction. Their phases were determined by deuterium contrast, using H_2O/D_2O exchange (20–22). Besides DOTAP/Cl^-, several equivalent samples containing (D3)DOTAP

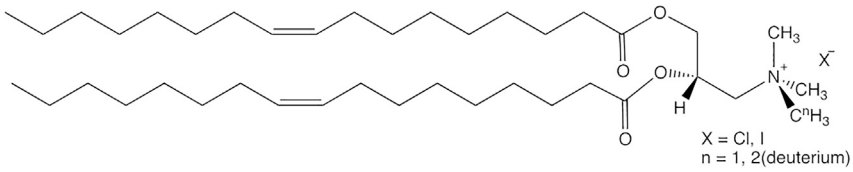

FIGURE 1 Structure of 1,2-dioleoyl-3-trimethylammonium propane (DOTAP).

were prepared, and each sample was measured in at least three H_2O/D_2O contrast conditions and three hydrations. Thus, redundant sets of structure factor differences ($\Delta F = F_h^D - F_h^H$, see Eq. 1) between deuterated and non-deuterated homologs (deuterium difference structure factors) were analyzed simultaneously to obtain the parameters of the deuterium (D3 and D_2O) distributions on an absolute scale, as described previously (20,22). Table 1 shows representative sets of structure factors that were used to determine the scattering length densities (SLD) presented in Fig. 2. SLDs were calculated according to the following equation:

$$SLD(z) = A_{lip}\sum_i w_i\rho_i + \frac{2}{d}\sum_h F_h \cos\left(\frac{2\pi\, h\, z}{d}\right) \quad (1)$$

The first term is the average SLD of the lipid and associated water, which can be described as a cylinder with cross-sectional area A_{lip} measured along the surface of the bilayer, and height $d/2$, measured along the z axis, where d is the repeat distance. All components of the bilayer (lipid, water, counterion) contribute their SLD (ρ_i) and their molar fraction (w_i). The second term of the equation describes the fluctuations in SLD about the average. The area per lipid (A_{lip}) varies dramatically with composition, hydration, or temperature. Therefore, all profiles are determined here on an "absolute-relative" scale that leaves A_{lip} undetermined (20). A Levenberg-Marquardt nonlinear least-squares fit was used, with χ^2 weighted by the uncertainties in the measured data (standard deviation, SD, due to counting statistics). Fit-parameter confidence intervals were determined by a Monte-Carlo resampling technique (20), where a large number ($n = 100$) of statistically independent sets of mock structure factor values (normally distributed within ± 1 SD) were tested, thus producing one set of fit parameters for each iteration. The means and SDs of the fit parameters were calculated from these sets.

X-ray diffraction measurements were performed on a Rigaku Smartlab (Rigaku Americas Corporation, The Woodlands, TX) diffractometer at the Institute for Bioscience and Biotechnology Research, Rockville, MD.

TABLE 1 Scaled Structure Factors for Neutron Diffraction from Oriented Multilayers of Unlabeled and Deuterated DOTAP/Cl⁻

[a](h)	[b]F(h) (H_2O)	[c]ΔF(h) (D_2O/H_2O)	[d]ΔF(h) (CD_3/CH_3)
1	−2.65 ± 0.10	−4.58 ± 0.42	−1.67 ± 0.08
2	−3.84 ± 0.14	2.61 ± 0.16	0.77 ± 0.12
3	2.76 ± 0.10	−0.96 ± 0.14	0.13 ± 0.09
4	−2.07 ± 0.08	0.21 ± 0.13	−0.62 ± 0.07
5	−0.62 ± 0.04	−0.15 ± 0.07	0.44 ± 0.06
6	0.83 ± 0.05	0.06 ± 0.08	−0.33 ± 0.07
7	0 ± 0.11	0 ± 0.16	0 ± 0.17
8	0 ± 0.10	0 ± 0.13	0 ± 0.18

[a]Diffraction index.
[b]Scaled structure factors for unlabeled DOTAP/Cl⁻, in H_2O. Uncertainties are 1 SD due to counting statistic and scaling (see materials and methods).
[c]The difference in neutron structure factors from a sample hydrated in a mixture D_2O/H_2O (1:4 M ratio) versus pure H_2O.
[d]The difference in neutron structure factors between a sample made from a (D3)DOTAP/DOTAP (1:2 M ratio) and a homologous sample made of DOTAP.

Phases of the structure factors were determined using the swelling method (23), when possible. Repeat spacings (d) and their uncertainties, calculated as the root mean squared deviations, for both neutron and x-ray diffraction, were determined by linear fitting of the Bragg peak positions versus diffraction index (h).

RESULTS

DOTAP/Cl⁻ dry films can be readily dispersed in water to produce stable vesicles, which can form multilayered lamellar phases alone or in mixture with DNA and helper lipids, such as DOPC (24,25), after allowing the bulk water to evaporate. Oriented multilayers (Fig. 2 *A*, inset), hydrated from the water vapor of saturated salt solutions, produce intense neutron diffraction from bilayer planes. Up to eight visible diffraction orders from the thermally disordered bilayers were visible (Fig. 2 *A*), depending on hydration and deuterium label position.

Replacement of some or all molecules in the sample with deuterium-labeled isoforms (H/D contrast variation) allowed determination of the positions of the deuterium atoms in the bilayer with tenths of an Ångström accuracy with virtually no perturbation to the original molecular structure (materials and methods). The strong changes in the diffraction signal (Fig. 2 *A*) when using deuterium oxide (D_2O) instead of H_2O, or deuterated DOTAP versus DOTAP, were translated into time- and ensemble-averaged spatial distributions of water molecules and deuterated groups projected onto the z axis. For each sample of DOTAP/Cl⁻, an equivalent sample was made using (D3)DOTAP/Cl⁻ that carries three deuterons on one of its methyl groups of the trimethylammonium (Fig. 2 *B*, inset). The D3 label was used to determine the profile of a methyl in the headgroup (HG) region. The combination of (D3) methyl and (D_2O) water labeling allowed for calibration of structure factors (Table 1) and calculation of the SLD profiles (Fig. 2 *B*) on an absolute scale up to a multiplication factor (A_{lip}) that accounts for the area per lipid, which is left undetermined (see materials and methods). Importantly, the $D3/D_2O$ labeling scheme was used to determine the number of waters associated with a DOTAP lipid headgroup for various hydration levels (Table 2).

The gradual uptake of water (swelling) in the DOTAP/Cl⁻ oriented multilayered samples, with increasing RH, is seen as both an increase in the repeat spacing (d) and in the full width at half maximum (*fwhm*) of the water profiles (Fig. 3 *A* and *B*; Table 2). Water is seen to accumulate in the HG region completely covering the ammonium group and reaching toward the carbonyl region of the two chains. By

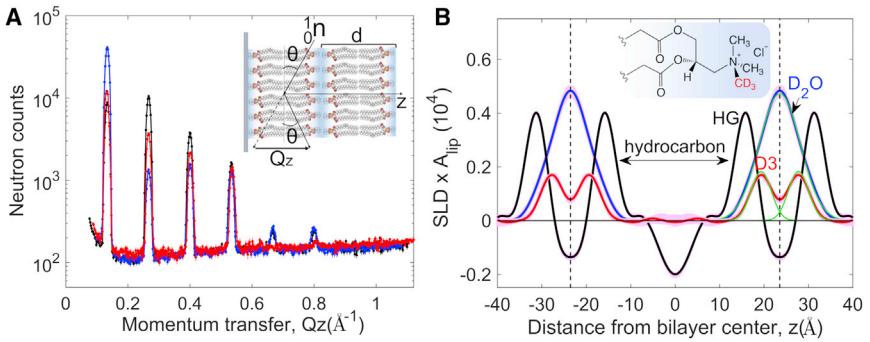

FIGURE 2 Neutron diffraction data from DOTAP/Cl$^-$ bilayers with deuterium labeling. (***A***) Representative, raw diffraction patterns from oriented bilayer stacks formed by DOTAP/Cl$^-$, probing the direction (z) normal to the bilayer surface: DOTAP/Cl$^-$ in H_2O (*black*), DOTAP/Cl$^-$ in H_2O/D_2O (4:1 M ratio) (*blue*), and (D3)DOTAP/DOTAP (1:2 M ratio) in H_2O (*red*). Inset shows the diffraction geometry. The data were obtained at 93% RH and 23°C. (***B***) The one-dimensional scattering length density profiles, projected on to the z axis, calculated from the data in (*A*). The profiles represent the bilayer structure (*black*), with high SLDs of the TMA headgroup surfaces bounding the lower SLD of the oleic chains (hydrocarbon region). Using deuterium (D = ^{2}H) as a contrast label against hydrogen the profiles of the deuterated methyl group (D3) (*red*) and the water (D_2O) were singled out. Pink bands are the calculated uncertainties in the profiles, as described in materials and methods. The D3 and D_2O profiles filling out the space between two adjacent bilayers can be described by Gaussian distributions (*green*), with the following positions and widths (*fwhm*): z (D3) = 19.4 ± 0.1 Å; *fwhm* (D3) = 5.4 ± 0.2 Å (for water profile values, see Table 2). The dotted vertical lines are used as delimiters of one repeat unit, d (e.g., one bilayer including the water of hydration) in the multilayer system (inset in *A*). d = 47.1 ± 0.1 Å for DOTAP/Cl$^-$ measured in H_2O, at 93% RH and 23°C. Various DOTAP/Cl$^-$ samples, measured under the same conditions, showed small variations (less than 0.5 Å) in the value of d. A_{lip} denotes area per lipid. The uncertainties represent 1 SD and were determined as described in materials and methods.

comparison, DOPC, which consists of the same oleic chains in the hydrocarbon, but carries an additional phosphate in the HG, displays a larger repeat spacing than DOTAP (by 4–5 Å) and a sharper increase in slope (d versus RH) at larger humidities (Fig. 3 *B*). Comparable trends were determined from x-ray diffraction measurements of oriented DOPC, where the break in the slope somewhere above 86% RH was interpreted as the point of completion of the hydration shell around the lipid HG (26).

The swelling capacity of zwitterionic, uncharged bilayers with the applied water vapor pressure is dictated primarily by the solvation repulsion (due to the orientation of water by the electric field surrounding the polar HG) and out of plane thermal fluctuations, which together constitute the main repulsive barrier for fluid spacing >5 Å (27). The fluctuations are reduced for charged bilayers at small separation distances (<30 Å) where the "hydration force" dominates (28).

Fig. 3 *C* shows the extent to which the presence of the phosphate group affects the profile of the bilayer and the water distribution. The neutron SLD profile is dominated by the carbonyl groups for a DOTAP/Cl$^-$ bilayer, and by the carbonyl and phosphate groups, together, for DOPC (29). The distance between the maxima in the bilayer profiles (d_{HG}) 31.7 Å (±0.1 Å) for DOTAP/Cl$^-$ and 32.1 Å (±0.1 Å) for DOPC (22) is representative of the hydrocarbon thickness of the bilayers and shows only a modest variation between the two lipids. However, the repeat distances (water-to-water peaks) are 47.1 Å for the DOTAP/Cl$^-$ bilayer (Table 2) and 51.6 Å for DOPC (22), for measurements at 93% RH. The significant increase of 4.5 Å in the repeat spacing from DOTAP/Cl$^-$ to DOPC is clearly due to the phosphate group and the additional water that it brings with it to the HG region rather than to changes in the hydrocarbon core thickness. Indeed, at this hydration level (93% RH), the number of water molecules per lipid is 6.5 for DOTAP/Cl$^-$ (Table 2) compared with 9.5 for DOPC (22,26). The three extra water molecules per DOPC must be in the form of water molecules associated with the phosphate group, which are lacking in DOTAP.

TABLE 2 Parameters Describing Water (D_2O) Profiles for DOTAP/Cl$^-$ Bilayers at Various Hydrations

Relative Humidity	Z (water) = d/2	FWHM (water)	[a]Nw
66%	22.9 ± 0.02	7.3 ± 0.4	3.0 ± 0.2
86%	23.1 ± 0.04	8.7 ± 0.2	4.4 ± 0.3
93%	23.6 ± 0.04	10.8 ± 0.9	6.5 ± 0.7

[a]Number of water molecules per lipid. The uncertainties represent 1 SD and were determined as described in materials and methods.

Note that the 0.5 Å larger d_{HG} for DOPC may simply be due to the phosphate group contribution shifting the maxima in the SLD profile and not necessarily to an increase in the hydrocarbon thickness. It is interesting that after careful scaling of the structure factors, using deuterium content for calibration, the resulting SLD profiles of DOTAP/Cl$^-$ and DOPC match well in the bilayer hydrocarbon center, an indication that the area per lipid (A_{lip}) must be very similar for the two lipids, at least under these measurement conditions. Similar differences between the two lipids were found for other hydrations.

In contrast to DOTAP/Cl$^-$, DOTAP/I$^-$ is not generally soluble in water. It was our experience that even after extensive agitation, heating, and sonication cycles, dry films of pure DOTAP/I$^-$ remained either stuck to the glass or dislodged as large, waxy particulates. However, a white suspension can be obtained with phosphate or HEPES buffers with sodium chloride salts. This suspension can form aligned lamellar samples when deposited on a glass coverslip, producing an intense diffraction pattern that stands out in x-ray diffraction measurements (Fig. 4 *A*), by

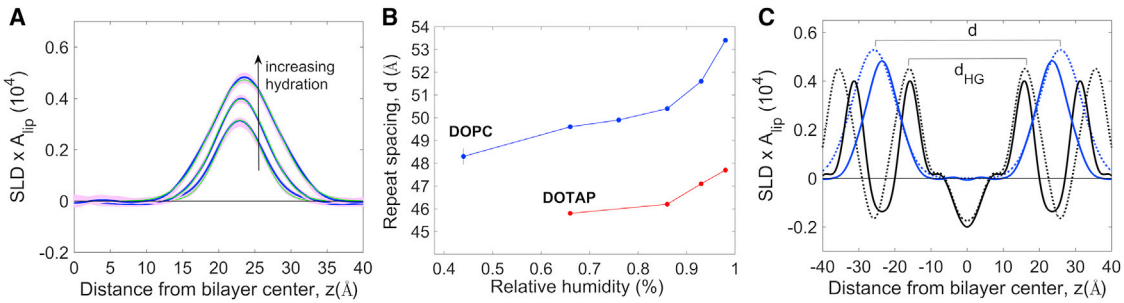

FIGURE 3 Hydration swelling of DOTAP/Cl^-. (***A***) The average water (D_2O) distribution (*blue*) in DOTAP/Cl^- multilayered lamellar samples hydrated from the water vapor at increasing relative humidities (66%, 86%, and 93%) and 23°C. Pink bands describe the uncertainties in the water profiles calculated as described in materials and methods. The water profiles can be described by Gaussian distributions (*green*) with positions at $z = d/2$ and *fwhm* given in Table 2. (***B***) A comparison between the repeat distance of the DOTAP/Cl^- and 1,2-dioleoyl-sn-glycero-3-phosphocholine (DOPC). Error bars are generally smaller than marker sizes and were determined as described in materials and methods. (***C***) Bilayer (*black*) and water profile (*blue*) for DOTAP (*solid lines*) and DOPC (*dotted lines*) for samples measured at 86% RH and 23°C.

comparison with that for neutron diffraction (Fig. 4 *A*, inset). Indeed, the exchange between Cl^- and I^- counterions does not produce a big change in the neutron scattering length (SL) of the trimethylammonium HG, although $SL(Cl) = 9.577 \times 10^{-5}$ Å is somewhat larger than $SL(I) = 5.280 \times 10^{-5}$ Å. However, it produces a dramatic difference for x-rays due to the more massive I^-. The presence of I^- as a x-ray contrast agent and the lack of thermal fluctuations in the absense of water give rise to a rigid crystalline multilayered structure that exhibits intense Bragg diffraction up to large scattering angles.

The one-dimensional diffraction pattern, probing the z direction, shows equidistant peaks corresponding to a repeat distance of around 53 Å, as expected for one bilayer thickness. Interestingly, the peak intensities display a "camel back" pattern, that goes through zero near the diffraction order ($n = 7$). This is indicative of the presence of the electron-dense I^- ion that dominates the bilayer structure factor and modulates the multilayer x-ray diffraction pattern though a decaying cosine function contribution, $ED\cos(n\,(d/2 - Z)\,2\pi/d)$, with an amplitude given by the electron density (ED) of iodide. The canceling of the cosine function near the ($n = 7$) position puts the iodide ion at $Z = 24.7$ Å from the bilayer center, for the repeat distance $d = 53.3$ Å (Fig. 4 *A*). Although contributions from other scattering centers (molecular groups) in the bilayer are present, they are small compared with that from I^- (e.g., $ED(I^-) = 1.28$ electrons/Å^3, $ED(H_2O) = 0.33$ electrons/Å^3, $ED(CH_2) = 0.29$ electrons/Å^3) (30).

Measurements of DOTAP/I^- samples at increasing humidity levels did not produce changes in the repeat spacing (no swelling). Similarly, when a DOTAP/I^- sample was measured by neutron diffraction in H_2O and D_2O, the Bragg intensities remained unchanged, a clear indication that no water was taken up by the lipid sample. The lack of swelling and change in structure factors with H_2O/D_2O contrast variation precluded a phase assignment of the neutron structure factors and calculation of the bilayer density profiles. Unlike DOTAP/Cl^-, which was found to mix well with DOPC (24), DOTAP/I^- was found here to segregate into a separate phase, with a larger bilayer thickness than that of the fluid DOPC (Fig. 4 *B*).

Overall, the x-ray and neutron diffraction data are consistent with the formation of two-dimensional I^- lattices along bilayer planes, through ionic bonds with the ammonium groups, and the displacement of water from the DOTAP/I^- HG.

DISCUSSION

DOTAP is a synthetic cationic lipid used in a broad range of applications, such as vaccine and anticancer drug formulations (31), as an adjuvant for immune response enhancement (32,33), and as a tool in electrophysiology studies (34). Despite the large amount of data that has been accumulated on DOTAP and related transfection molecules, many aspects of cationic lipid transfection remain unclear (7). The influence of halide counterions on the structure and hydration of DOTAP merit careful consideration because this may ultimately dictate how LNPs incorporating DOTAP or its derivatives will interact with both the oligonucleotide cargo and the cellular membrane target. Of particular interest are the halide ions I^- and Cl^-, which are often used interchangeably in the constitution of LNPs. Although it has been found that gene transfection can be considerably affected by the two counterions (7,11), trends in the results vary. This variability can be explained if different amounts of exchange from DOTAP/I^- to Cl^- occur during sample preparations in buffers containing chloride salts at various concentrations. However, from the start, the choice of using iodinated forms of the cationic lipids for in vitro and in vivo transfection studies (9,12,13) is surprising, given the poor solubility of these lipids in water-based solutions, alone or in combination with other (helper) lipid components such as POPE, cholesterol, or DOPC ((11), this work). One reason for using iodinated variants could, presumably, be for controlling surface hydration of LNPs, which has been acknowledged to be an important factor in the fusion of the LNPs with target cellular membranes (8). To clarify

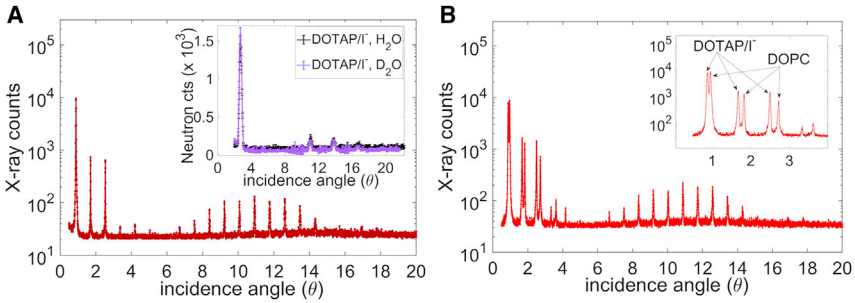

FIGURE 4 DOTAP/I^- diffraction data. (*A*) Using I^- counterion instead of Cl^- leads to the formation of crystalline structure, and intense x-ray diffraction pattern modulated by the presence of the massive iodide ion (*red*). The tight binding of I^- in the $DOTAP^+$ trimethyl-ammonium headgroup causes a complete dehydration of the bilayer, seen here as an unchanged neutron diffraction signal upon solvent (H_2O/D_2O) contrast variation (inset). The repeat spacing is $d = 53.3 \pm 0.4$ Å. (*B*) Mixtures (1:1 M) of DOTAP/I^- with DOPC lead to separation of the two lipids in domains of differing repeat spacings, $d = 53.1 \pm 0.3$ Å for DOTAP/I^- and 50.9 ± 0.1 Å for DOPC, measured at 93% RH and 23°C. Note that, compared with DOTAP/I^-, the signal from the DOPC multilayers fades quickly after the fourth diffraction order (inset is a zoomed in view on diffraction orders 1–4), a common feature of thermally disordered bilayers. The uncertainties represent 1 SD and were determined as described in materials and methods.

the hydration issue, it is important to understand the basic structure of DOTAP bilayers by themselves. Here, with neutron diffraction and deuterium labeling, we were able to examine and quantify a few important structural features of DOTAP bilayer with Cl^- and I^- counterions.

We found that DOTAP/Cl^- readily self-assembles into bilayers in pure water, displaying a polar headgroup that can take up water despite the absence of the phosphate moiety. The hydration layer extends past the ammonium group into the glycerol-carbonyl region (Fig. 3 *B*), and it shows swelling behaviors similar to that of PC lipids (19), albeit at a slower rate. At membrane separations between 5 and 20 Å (as it is the case here), the swelling of electrically charged multilayers was shown to be dominated by a repulsive "hydration force" that overwhelms electrostatic repulsion and opposes the van der Waals attraction (28). Screening of the electrostatic repulsion between bilayers by counterions attached to the lipid HG is expected to make the repulsive hydration force even stronger compared with the electrostatic component. Thus, the hydration force may preclude fusion of LNPs containing cationic lipids like DOTAP with membranes and therefore likely to be an important factor in transfection.

We also found that, compared with DOTAP/Cl^-, DOPC carries three additional water molecules with it in bilayers, which are water molecules associated with the phosphate moiety. The lipid phosphate group is a key structural feature that readily forms hydrogen bonds with water and neighboring lipids, thus increasing bilayer stability, to which addition of DOTAP/Cl^- may act as a destabilizer. The phosphates were also shown to be essential in coupling with arginine residues of voltage-gated ion channels (6,35) and enabling movement of the voltage sensors through the bilayer, since exchange of PC lipids for DOTAP affects the channel activity by promoting the "resting" state (34).

Although DOTAP/I^- is insoluble in pure water under normal condition, it can be forced into a turbid suspension in sodium chloride salt solutions by itself or in mixture with DOPC. However, when multilayers are produced and examined by diffraction methods, the resulting DOTAP multilayers retain the I^- ion. This indicates that, under normal buffer and pH conditions, DOTAP prefers remaining bound to the iodide even in the presence of Cl^- ions in solution. The halide ions were shown to bind from aqueous solutions to bilayers containing DOTAP, with affinities that follow the Hofmeister sequence: $I^- >> Br^- > Cl^-$ (36,37). Binding experiments indicated that I^- exhibits significantly stronger interaction with the cationic membranes than Cl^- and Br^- and that the interaction is primarily electrostatic in nature (37). Our results are consistent with the finding that the affinity to cationic lipid membranes is much larger for I^- than Cl^-. For dioctadecyl-dimethylammonium (DODA), another lipid with a quaternary ammonium ion headgroup, Woiterski et al. (38) used attenuated total reflection Fourier transform infrared spectroscopy to find 11 water molecules bound per DODA/F^-, 1–2 water molecules per DODA/Cl^- and DODA/Br^-, and no water bound to DODA/I^-.

Our neutron diffraction data with H_2O/D_2O contrast variation clearly demonstrates that there is no water associated with the DOTAP/I^- bilayers. However, the much larger repeat distance (by ~ 6 Å) displayed by a dehydrated DOTAP/I^-, compared with a hydrated DOTAP/Cl^- measured under the same conditions, must be due to a significant thickening of the hydrocarbon core of DOTAP/I^- compared with that of DOTAP/Cl^-. At constant hydrocarbon density, this thicker hydrocarbon core results from a much tighter lipid packing, which suggests that the I^- acts as a ligand, possibly coordinating a few lipid HGs across the bilayer plane. Crystal structures of molecules containing hydrophobic regions and trimethylammonium-iodide indicate that the I^- ion coordinates up to four TMA^+ ions arranged tetrahedrally with N^+– I^- distances of 4.5 Å to 4.8 Å (39–42), where short distances are limited by the steric hindrance of methyl groups of radius 2.0 Å (43) and a methylene group, which form the tetrahedral planes, plus the 2.2 Å radius of the iodide ion (44). For DOTAP/I^- bilayers, a likely arrangement has an I^- ion coordinated by TMA^+ groups from two adjacent bilayers, thus cross-linking the two bilayers. The ionic interactions should be stronger than hydration interactions because of ideal geometric conditions and the high polarizability of the I^- (45) and TMA^+ (46) ions. Therefore, water would not change the

composition or the structure of the bilayers, as indicated by our neutron diffraction data (Fig. 3 *A*, inset).

Finally, when mixed, together, DOPC and DOTAP/I^- separate away from each other into domains with different physical and chemical properties. Based on our data, the lipid separation can be explained by the different hydration properties and the dramatic mismatch in both the headgroup sizes and hydrocarbon thicknesses.

CONCLUSION

The performance of a cationic lipid in drug delivery depends strongly on the types of counterions present that affect the structure, hydration, and mixing with other lipids. The tight attachment of I^- to DOTAP's TMA^+ headgroups would, presumably, hinder the binding of nucleic acids, making DOTAP/I^- unsuitable for LNP formulations. The insolubility issue of DOTAP/I^- and its tendency to segregate away from "helper" lipids commonly used in LNPs requires careful consideration and reassessment. Particularly, in forming LNPs using DOTAP/I^-, one can expect the fraction of incorporated DOTAP/I^- to be smaller than intended. A careful quantification of the incorporated components is, generally, not done in practice. Furthermore, the combination of DOTAP/I^- with helper lipids may likely lead to segregation of lipid components into domains and aggregation of lipid vesicles though the cross-linking ability of I^-, which in itself can affect the transfection profiles of LNPs.

AUTHOR CONTRIBUTIONS

M.M., D.L.W., and S.H.W. designed the research. C.L.C. and A.R.C. did the chemical synthesis. M.M. and D.L.W. performed diffraction measurements and analyzed the data. All authors contributed to writing the article.

ACKNOWLEDGMENTS

This work was supported in part by US National Institutes of Health grants RO1 GM74737 and R35 GM139652 from NIGMS; Program Project GM86685 from the NIGMS and NINDS (S.H.W., D.T., R.C). We are grateful for the support of the National Institute of Standards and Technology, US Department of Commerce, in providing the neutron research facilities used for neutron diffraction experiments. The identification of any commercial product or trade name does not imply endorsement or recommendation by the US National Institute of Standards and Technology. We are pleased to dedicate this paper to our distinguished colleague and friend of many years, Dr. Klaus Gawrisch.

DECLARATION OF INTERESTS

The authors declare no competing interests.

REFERENCES

1. Hou, X., T. Zaks, …, Y. Dong. 2021. Lipid nanoparticles for mRNA delivery. *Nat. Rev. Mater.* 6:1078–1094. https://doi.org/10.1038/s41578-021-00358-0.
2. Yonezawa, S., H. Koide, and T. Asai. 2020. Recent advances in siRNA delivery mediated by lipid-based nanoparticles. *Adv. Drug Deliv. Rev.* 154-155:64–78. https://doi.org/10.1016/j.addr.2020.07.022.
3. Felgner, P. L., T. R. Gadek, …, M. Danielsen. 1987. Lipofection - a highly efficient, lipid-mediated DNA-transfection procedure. *Proc. Natl. Acad. Sci. USA.* 84:7413–7417. https://doi.org/10.1073/pnas.84.21.7413.
4. Stamatatos, L., R. Leventis, …, J. R. Silvius. 1988. Interactions of cationic lipid vesicles with negatively charged phospholipid vesicles and biological membranes. *Biochemistry.* 27:3917–3925.
5. Zheng, H., W. Liu, …, Q. X. Jiang. 2011. Lipid-dependent gating of a voltage-gated potassium channel. *Nat. Commun.* 2:250. https://doi.org/10.1038/ncomms1254.
6. Andersson, M., J. A. Freites, …, S. H. White. 2011. Structural dynamics of the S4 voltage-sensor helix in lipid bilayers lacking phosphate groups. *J. Phys. Chem. B.* 115:8732–8738.
7. Simberg, D., S. Weisman, …, Y. Barenholz. 2004. DOTAP (and other cationic lipids): chemistry, biophysics, and transfection. *Crit. Rev. Ther. Drug Carrier Syst.* 21:257–317. https://doi.org/10.1615/CritRevTherDrugCarrierSyst.v21.i4.10.
8. Zhi, D., S. Zhang, …, D. Zhao. 2013. The headgroup evolution of cationic lipids for gene delivery. *Bioconjugate Chem.* 24:487–519. https://doi.org/10.1021/bc300381s.
9. Aberle, A. M., M. J. Bennett, …, M. H. Nantz. 1996. The counterion influence on cationic lipid-mediated transfection of plasmid DNA. *Biochim. Biophys. Acta.* 1299:281–283. https://doi.org/10.1016/0005-2760(95)00230-8.
10. Kim, Y. J., T. W. Kim, …, S. Y. Jeong. 2001. Counterion effects on transfection activity of cationic lipid emulsion. *Biotechnol. Bioproc. Eng.* 6:279–283. https://doi.org/10.1007/BF02931990.
11. Chen, H., H. Zhang, …, X. Guo. 2012. Novel pH-sensitive cationic lipids with linear ortho ester linkers for gene delivery. *Eur. J. Med. Chem.* 52:159–172. https://doi.org/10.1016/j.ejmech.2012.03.013.
12. Zhi, D., S. Zhang, …, D. Zhao. 2012. Synthesis and biological activity of carbamate-linked cationic lipids for gene delivery in vitro. *Bioorg. Med. Chem. Lett.* 22:3837–3841.
13. Gupta, K., S. J. Mattingly, …, B. A. Shapiro. 2015. Oxime ether lipids containing hydroxylated head groups are more superior siRNA delivery agents than their nonhydroxylated counterparts. *Nanomedicine.* 10:2805–2818. https://doi.org/10.2217/nnm.15.105.
14. Leventis, R., and J. R. Silvius. 1990. Interactions of mammalian-cells with lipid dispersions containing novel metabolizable cationic amphiphiles. *Biochim. Biophys. Acta.* 1023:124–132. https://doi.org/10.1016/0005-2736(90)90017-i.
15. Andresen, T. L., S. S. Jensen, …, K. Jørgensen. 2005. Synthesis and biological activity of anticancer ether lipids that are specifically released by phospholipase A(2) in tumor tissue. *J. Med. Chem.* 48:7305–7314. https://doi.org/10.1021/jm049006f.
16. Schmid, C. R. 2002. (4R)-2,2-Dimethyl-1,3-dioxolane-4-carboxaldehyde. *In* Encyclopedia of Reagents for Organic Synthesis.
17. Dunlap, N. K., J. Drake, …, L. Martin. 2008. Concise synthesis of enantiomers of 4-aminobutane-1,2,3-triol. *J. Org. Chem.* 73:2928–2930. https://doi.org/10.1021/jo702647n.
18. Dura, J. A., D. J. Pierce, …, S. H. White. 2006. AND/R: a neutron diffractometer/reflectometer for investigation of thin films and multilayers for the life sciences. *Rev. Sci. Instrum.* 77:074301.
19. White, S. H., R. E. Jacobs, and G. I. King. 1987. Partial specific volumes of lipid and water in mixtures of egg lecithin and water. *Biophys. J.* 52:663–665.
20. Wiener, M. C., G. I. King, and S. H. White. 1991. Structure of a fluid dioleoylphosphatidylcholine bilayer determined by joint refinement of x-ray and neutron diffraction data. I. Scaling of neutron data and the distribution of double-bonds and water. *Biophys. J.* 60:568–576.
21. Worcester, D. L., and N. P. Franks. 1976. Structural analysis of hydrated egg lecithin and cholesterol bilayers. II. Neutron diffraction. *J. Mol. Biol.* 100:359–378.

22. Mihailescu, M., R. G. Vaswani, …, S. H. White. 2011. Acyl-chain methyl distributions of liquid-ordered and -disordered membranes. *Biophys. J.* 100:1455–1462. https://doi.org/10.1016/j.bpj.2011.01.035.

23. Blaurock, A. E. 1971. Structure of nerve myelin membrane - proof of low-resolution profile. *J. Mol. Biol.* 56:35–52. https://doi.org/10.1016/0022-2836(71)90082-9.

24. Safinya, C. R. 2001. Structures of lipid-DNA complexes: supramolecular assembly and gene delivery. *Curr. Opin. Struct. Biol.* 11:440–448. https://doi.org/10.1016/s0959-440x(00)00230-x.

25. Salditt, T., I. Koltover, …, C. R. Safinya. 1997. Two-dimensional smectic ordering of linear DNA chains in self-assembled DNA-cationic liposome mixtures. *Phys. Rev. Lett.* 79:2582–2585. https://doi.org/10.1103/PhysRevLett.79.2582.

26. Hristova, K., and S. H. White. 1998. Determination of the hydrocarbon core structure of fluid dioleoylphosphocholine (DOPC) bilayers by x-ray diffraction using specific bromination of the double-bonds: effect of hydration. *Biophys. J.* 74:2419–2433.

27. McIntosh, T. J., A. D. Magid, and S. A. Simon. 1989. Repulsive interactions between uncharged bilayers - hydration and fluctuation pressures for monoglycerides. *Biophys. J.* 55:897–904. https://doi.org/10.1016/s0006-3495(89)82888-7.

28. Cowley, A. C., N. L. Fuller, …, V. A. Parsegian. 1978. Measurement of repulsive forces between charged phospholipid bilayers. *Biochemistry.* 17:3163–3168.

29. Wiener, M. C., and S. H. White. 1992. Structure of a fluid dioleoylphosphatidylcholine bilayer determined by joint refinement of x-ray and neutron diffraction data. III. Complete structure. *Biophys. J.* 61:434–447.

30. Warren, B. E. 1969. X-Ray Diffraction. Addison-Wesley, Reading, MA.

31. Berlin Grace, V., and S. Viswanathan. 2017. Pharmacokinetics and therapeutic efficiency of a novel cationic liposome nano-formulated all trans retinoic acid in lung cancer mice model. *J. Drug Deliv. Sci. Technol.* 39:223–236. https://doi.org/10.1016/j.jddst.2017.04.005.

32. Ma, Y., Y. Zhuang, …, L. Cai. 2011. The role of surface charge density in cationic liposome-promoted dendritic cell maturation and vaccine-induced immune responses. *Nanoscale.* 3:2307–2314. https://doi.org/10.1039/c1nr10166h.

33. Mansury, D., K. Ghazvini, …, M. R. Jaafari. 2019. Increasing cellular immune response in liposomal formulations of DOTAP encapsulated by fusion protein hspx, PPE44, and esxv, as a potential tuberculosis vaccine candidate. *Rep. Biochem. Mol. Biol.* 7:156–166.

34. Zheng, H., W. Liu, …, Q.-X. Jiang. 2011. Lipid-dependent gating of a voltage-gated potassium channel. *Nat. Commun.* 2:250–259.

35. Krepkiy, D., M. Mihailescu, …, K. J. Swartz. 2009. Structure and hydration of membranes embedded with voltage-sensing domains. *Nature.* 462:473–479.

36. Pokorna, S., P. Jurkiewicz, …, M. Hof. 2013. Interactions of monovalent salts with cationic lipid bilayers. *Faraday Discuss.* 160:341–358. discussion 389-403. https://doi.org/10.1039/c2fd20098h.

37. Maity, P., B. Saha, …, S. Karmakar. 2018. Effect of zwitterionic phospholipid on the interaction of cationic membranes with monovalent sodium salts. *Langmuir.* 34:9810–9817. https://doi.org/10.1021/acs.langmuir.8b01792.

38. Woiterski, L., D. W. Britt, …, C. Selle. 2012. Oriented confined water induced by cationic lipids. *Langmuir.* 28:4712–4722. https://doi.org/10.1021/la205043x.

39. Zanotti, G., A. Delpra, …, S. García-Blanco. 1977. Ttereochemistry of muscarinic antagonists .1. Crystal and molecular-structure of (2-diphenylaminoethyl)trimethylammonium iodide. *Acta Crystallogr. B.* 33:3006–3010. https://doi.org/10.1107/s0567740877010152.

40. Gieren, A., and M. Kokkinidis. 1986. Structure investigations of agonists of the natural neurotransmitter acetylcholine. 4. x-ray structure analyses of trimethylpentylammonium-chloride and (4-Acetoxybutyl) Trimethylammonium-iodide. *Z. Naturforsch., C: J. Biosci.* 41:618–626.

41. Gabe, E. J., and D. F. Grant. 1962. Crystal structure of menthyl trimethylammonium iodide. *Acta Crystallogr.* 15:1074–1077. https://doi.org/10.1107/s0365110x62002893.

42. Barlow, R. B., O. Johnson, …, G. Koellner. 1989. A comparison of the crystal-structures of some quaternary trimethylammonium salts related to dopamine and noradrenaline with those of the corresponding amines - a comment on their nicotine-like biological activities. *Acta Crystallogr.* B45 (Pt 4):396–404. https://doi.org/10.1107/s0108768189002740.

43. Shannon, R. D. 1976. Revised effective ionic-radii and systematic studies of interatomic distances in halides and chalcogenides. *Acta Crystallogr. A.* 32:751–767. https://doi.org/10.1107/s0567739476001551.

44. Pauling, L., and D. C. Carpenter. 1936. The crystal structure of metaldehyde. *J. Am. Chem. Soc.* 58:1274–1278. https://doi.org/10.1021/ja01298a054.

45. Jaswal, S. S., and T. P. Sharma. 1973. Electronic polarizabilities of ions in alkali-halide crystals. *J. Phys. Chem. Solid.* 34:509–511. https://doi.org/10.1016/0022-3697(73)90045-0.

46. Ritchie, G. L. D., and E. W. Blanch. 2003. Temperature dependence of the electrooptical Kerr effect: anisotropic electric dipole polarizabilities of NH3, CH3NH2, (CH3)(2)NH,and (CH3)(3)N. *J. Phys. Chem. A.* 107:2093–2099. https://doi.org/10.1021/jp0223152.